SOFT ROBOTICS
Volume 00, Number 00, 2020

DOI: 10.1089/soro.2019.0066

SoRo
Soft Robotics

Untethered Soft Robotics with Fully Integrated Wireless Sensing and Actuating Systems for Somatosensory and Respiratory Functions

Byungkook Oh,[1,2,*] Young-Geun Park,[1,2,*] Hwaebong Jung,[1,*] Sangyoon Ji,[1,2,*] Woon Hyung Cheong,[1,2] Jinwoo Cheon,[2] Wooyoung Lee,[1] and Jang-Ung Park[1,2]

Abstract

There has been a great deal of interest in designing soft robots that can mimic a human system with haptic and proprioceptive functions. There is now a strong demand for soft robots that can sense their surroundings and functions in harsh environments. This is because the wireless sensing and actuating capabilities of these soft robots are very important for monitoring explosive gases in disaster areas and for moving through contaminated environments. To develop these wireless systems, complex electronic circuits must be integrated with various sensors and actuators. However, the conventional electronic circuits based on silicon are rigid and fragile, which can limit their reliable integration with soft robots for achieving continuous locomotion. In our study, we developed an untethered, soft robotic hand that mimics human fingers. The soft robotic fingers are composed of a thermally responsive elastomer composite that includes capsules of ethanol and liquid metals for its shape deformation through an electrothermal phase transition. And these soft actuators are integrated fully with flexible forms of heaters, with pressure, temperature, and hydrogen gas sensors, and wireless electronic circuits. Entire functions of this soft hand, including the gripping motion of soft robotic fingers and the real-time detections of tactile pressures, temperatures, and hydrogen gas concentrations, are monitored or controlled wirelessly using a smartphone. This wireless sensing and actuating system for somatosensory and respiratory functions of a soft robot provides a promising strategy for next-generation robotics.

Keywords: soft robotics, soft actuators, wireless sensors, multiplexed sensors

Introduction

Hard actuators comprise the rigid forms of materials and the components of various devices. While hard robotics systems can function in harsh environments and lift various objects, they have serious issues related to their weight, volume, high fabrication costs, and the high energy input required to initiate their locomotion. However, in recent years, there have been significant efforts to develop soft robotics that can overcome these issues.[1] Many of the reported soft robots can initiate multiple, sophisticated, and soft continuum motions, grasping motions like the hand of human being,[2] and they can be used in biological and biocompatible applications by designing the fully soft body frame of actuators.

However, to date, the pneumatic soft actuators[3–6] and electroactive actuators[7,8] require either pressure regulators or power sources through their wired connections. These tethered systems are limited in their ability to travel to unstructured surroundings,[9] as is the case in the biomedical[10] and biological fields.[11,12] In addition to the electroactive and pneumatic soft robotics, the actuation of some of the existing robotic models can be initiated using light[13,14] or magnetic fields.[15–17] Although soft robots that use photonic or magnetic waves can achieve their shape transitions without any tethered connection, such an external stimulus has challenges for conformal actuation and delicate motions due to the difficulty in the localization of these waves in soft robotic bodies.

[1]Department of Materials Science and Engineering, Nano Science Technology Institute, Yonsei University, Seoul, Republic of Korea.
[2]Center for Nanomedicine, Institute for Basic Science (IBS), Seoul, Republic of Korea.
*These authors contributed equally to this work.

In contrast to photonic or magnetic waves, the electric stimulus can flow along electrode patterns, which can be advantageous to the delicate motions of soft actuators. Among electrically actuatable soft materials, electroactive polymer composites, which include electrolytes that migrate along the direction of the electric field, can cause their shape transitions. However, these composites require high voltages (>1 kV) to initiate their actuations, which can limit their integration with conventional wireless circuits because the onboard power charging and supplying unit becomes bulky.[18,19] In contrast, the electrothermally responsive soft actuators have the advantage of lower driving voltages[20–24] (Supplementary Table S1). However, there is still the challenge of integrating electric circuits with these soft actuatable materials because conventional silicon-based (Si-based) electronic circuits and sensors for wireless real-time sensing and actuating systems are too rigid and fragile to restrain the sophisticated, multiform, and continuous motions of soft robots.[25–27]

Herein, we present an untethered, soft robotic hand that mimics human fingers using the electrothermal phase transition of a soft elastomeric actuator with its full integration with flexible heaters; multiple sensors for monitoring tactile pressures, temperatures, and hydrogen gas concentrations; and wireless electronic circuits, including a Bluetooth module, power charging and supplying units, and current amplifiers. As the soft actuatable material for finger motions, microcapsules of ethanol and liquid metals are dispersed together inside a silicone elastomer matrix. The vaporization of the ethanol in the microcapsules magnifies the expansion of the volume of the matrix, and the liquid metals in the microcapsules increase the thermal conductivity of the matrix. The attachment of a flexible Joule-heating film to this soft actuating layer enables its electrothermal phase transition by bending the bimorph to the desired curvature for gripping objects.

Two different structures of flexible, top-gated Si transistors (with or without elastomeric spacers) were fabricated using ultrathin Si nanomembranes (thickness: 300 nm) for the somatosensory system. Both transistors contain local air gaps as dielectrics (between Si and top-gate) to present high transconductance, and due to the clean interface between the Si channel and air, they have negligible hysteresis in their voltage–current characteristics. For sensing tactile pressures, the height of the air dielectric layers can be determined by the thickness of the elastomeric spacers between the Si and the top-gate, and their height can be decreased by applying pressure as the capacitance of the metal–air–Si structure increases. This pressure-sensitive change in capacitance enables an individual transistor to act solely as a single pressure sensor with a wide detection range from 200 Pa to 5 MPa. Also, another Si transistor with no elastomeric spacer can act as a temperature sensor by using the thermoresistive effect of Si.

For the respiratory system, a hydrogen gas sensor that consists of vertically oriented SnO_2 nanorod (NR) arrays was integrated into the soft robotic hand, and it can detect concentrations as low as 1 ppm. All electric signals from these three sensors, as well as the actuation bias for the soft robotic fingers, can be transmitted wirelessly or controlled through Bluetooth. Here, the rigid components of the hydrogen gas sensor, wireless circuit, and battery are integrated into the rigid back of the robotic hands (instead of the soft fingers) where no actuation occurs. Therefore, the motions of the soft fingers are not disturbed. The entire functions of this soft hand, including the real-time sensing capabilities and the gripping motion of the soft robotic fingers, are controlled wirelessly using a smartphone, which suggests that it offers substantial promise as a next-generation interface of soft robotics with smart sensors.

Materials and Methods

Fabrication of finger-like and hand-like soft actuators

The finger-like soft actuator (length: 8 cm, width: 2 cm) was constructed from three electrothermally responsive soft actuator segments. To electrothermally activate each segment of a soft robotic finger, we used a photolithography process to design a heater film, which was 8 cm long and 2 cm wide and had a customized mask. Three electrothermally responsive soft actuators and diced glasses as a joint were attached to a flexible heater film by applying a silicone adhesive (Ecoflex 5). A soft robotic hand was constructed from four soft robotic fingers and the main body. The main body was produced using the elastomer poly(dimethylsiloxane) (PDMS, Sylgard 184; Dow Corning Co.) and a 3D-printed mold. Actuation of each soft robotic finger was initiated by applying heat energy that was generated by electrical fields.

The measurement of contact force from individual soft robotic fingers

The contact force is measured using a force gauge (Mark-10, ESM303). After the actuation is initiated, the soft robotic finger is contacted directly at the force gauge pad. When the soft robotic finger pushes the force gauge, the contact force is delivered to the force gauge. Afterward, the force is displayed on the screen of the force gauge display. Supplementary Figures S1 and S2 show a photograph of the force gauge equipment and the relevant schematic illustrations on this measurement.

Integration of circuit boards

We used 10 circuit boards (4 LED current jumpers, a Beetle BLE—Arduino Bluetooth 4.0, three batteries, a customized sensor module, Bluetooth module) to wirelessly activate our hand-like soft actuator and sense the physics contact and harmful gases. To minimize the dimensions of the power charging and supplying unit, we mostly used the patterned heater at low power (5.14 W). The modules were integrated above the surface of the elastomeric body (PDMS) isolated from our soft robots.

Characterization of the output current of each sensor

We measured the characteristic output current of each sensor using the probe station equipment (Keithley 4200-SCS) by setting specific conditions, that is, a gate voltage of 25 V and a drain of 7 V.

Thermal images of activating the soft robotic fingers

Electrical current streams through the entire body of the soft actuator and thermal images heaters of the soft robotic fingers were visualized about joule heating. We optimized the emissivity of the heater film with 0.9. The thermal images of

the heater film reflected the temperature as it ranged from room temperature to 150°C. The images were captured by an IR camera (T650sc; FLIR systems, Wilsonville, OR). The distribution of the temperature throughout the surface of the soft robot was analyzed using the FLIR software (Research IR Max; FLIR Systems).

Results

Vaporization of the active liquid dispersed inside an elastomeric matrix can expand the volume of this elastomer significantly, which can form a soft material that is actuatable by controlling temperature. In our study, ethanol (boiling temperature: 78.4°C) was used as an active liquid with high vapor pressure, and it simply was mixed with a silicone elastomer (Ecoflex 00-30). The details of this fabrication are described in the Fabrication of a Single Soft Actuator section in the Supplementary Data. By supplying heat energy to increase the temperature of this elastomeric matrix to vaporize the ethanol rapidly, the internal pressure of the elastomeric matrix and the volume of the soft actuator are increased. This soft actuator can change its volume reversibly from its initial shape to the expanded condition and back to the initial shape because cooling transforms the ethanol from the gas phase to the liquid phase. However, the relatively low thermal conductivity of this elastomer, as well as the random dispersion of ethanol, can result in a slow thermal-response time and poor uniformity in the direction of the deformation of this soft actuator.[28]

To overcome these challenges, microcapsules of a liquid metal were dispersed along with ethanol inside the elastomeric matrix to increase its thermal conductivity[29] (Fig. 1a). In our study, eutectic gallium–indium alloy (EGaIn, 75.5% gallium, 24.5% indium alloy by weight) was used as the liquid metal. Contrast to the solid phase of thermally conductive nanomaterials,[30] this liquid metal can be stretched into the actuating direction without obstructing the actuation due to its high deformability with low stiffness. Then, a thin polyimide (PI) film (thickness: 50 μm) was attached to the top surface of this elastomer, where ethanol and EGaIn were dispersed together. The thermal expansion of this elastomeric matrix was significantly larger than the PI case, which can lead to the thermal bimorph bending as a soft actuator. As an example, Figure 1b presents photographs that show this bending at 100°C. The dispersion conditions of ethanol and EGaIn inside the elastomeric matrix were examined using microcomputed tomography, and Figure 1c shows that the microcapsules of these two different materials were dispersed uniformly inside this elastomer. The average diameters of the ethanol and EGaIn capsules were 300 and 10 μm, respectively (Supplementary Fig. S3).

Figure 1d shows the changes in the temperatures over time with different volume fractions of EGaIn. The heat dissipation

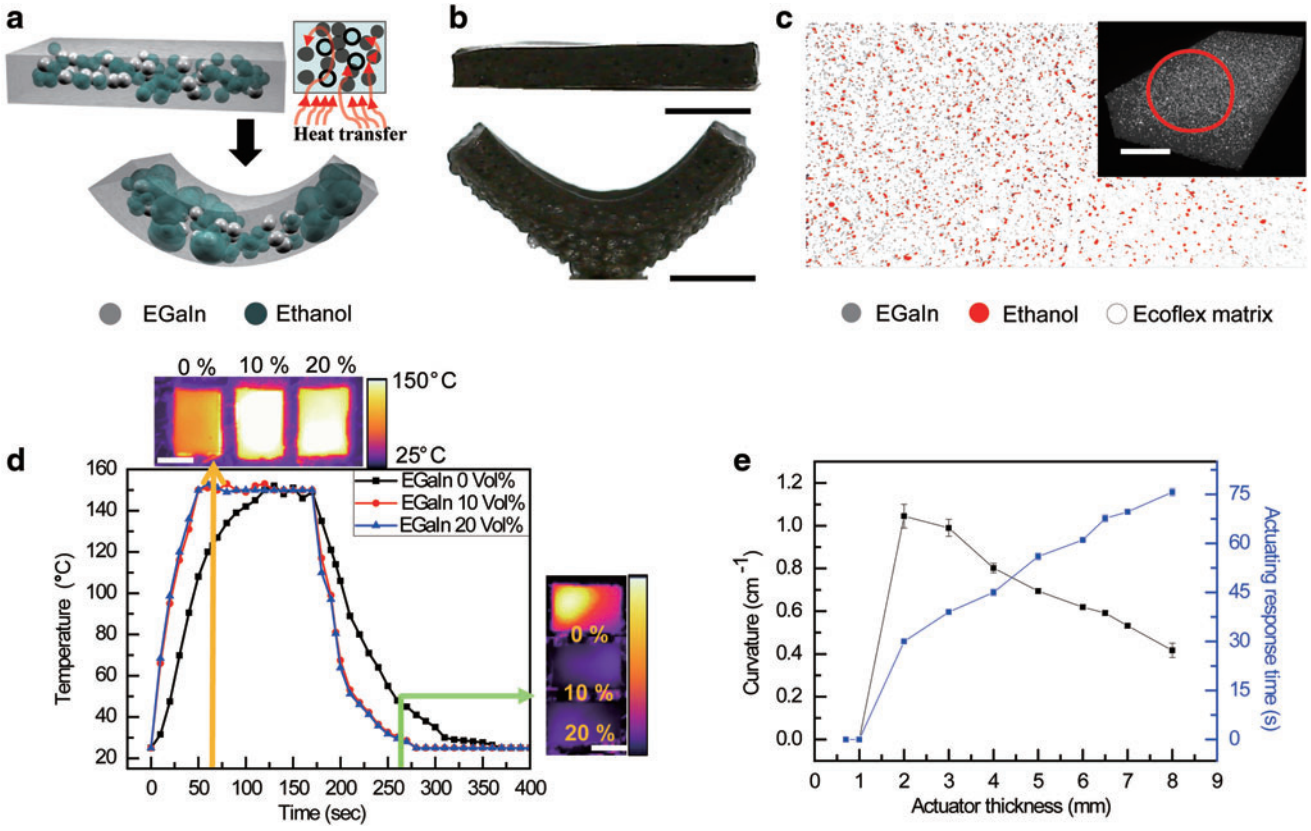

FIG. 1. Properties of soft actuating materials. **(a)** The schematic illustration of actuating mechanism. **(b)** Photographs of the actuation of thermal-responsive soft actuator. Scale bars, 10 mm. **(c)** The microcomputed tomography image of the soft actuator composite in the red circle of inset image. The red circle indicates the scanned regions using microcomputed tomography for obtaining 2D images. Scale bar, 10 mm. **(d)** The plot of temperature versus time of actuating materials with different volume fractions of EGaIn. Scale bars, 10 mm. **(e)** The soft actuator's properties optimized by the curvature and response time versus the actuator's thickness. EGaIn, eutectic gallium–indium alloy. Color images are available online.

and cooling rates of this elastomer were dependent on the volume fraction of EGaIn. In this study, the elastomer samples at room temperature with different contents of EGaIn were placed on the surface of a hot plate that was preheated to 150°C, and the temperature changes of these samples were monitored using the IR camera (T650sc; FLIR systems), as shown in Figure 1d. Although the temperatures of all the sample eventually reached 150°C, the temperatures of the samples that contained higher fractions of EGaIn increased faster. Their cooling rates also were compared, and it was observed that the samples that had higher fractions of EGaIn had a faster cooling rate. Thus, the higher fractions of EGaIn, which can increase the thermal conductivity of the elastomer matrix, are advantageous for faster bending motions of this soft actuator with relatively rapid expansion and contraction of the volumes.

Figure 1e shows that the curvature of bending and the response time of this soft actuator also were dependent on its thickness. The elastomeric composites were formed with thicknesses from 0.5 to 8 mm before attaching a 50-μm-thick PI film on its top surface for the thermal bimorph bending motions. The response time at 100°C increased with the thickness of this elastomer, which caused slower bending. The soft actuator sample with its thickness of 2 mm presented the highest bending curvature as well as the fastest response time. For the thickness below 1 mm, its thermal bimorph bending was not significant because the ethanol content was not sufficient for inducing its shape transition. The soft, 2-mm-thick actuator sample presented the highest bending curvature as well as the fastest response time. For thicknesses less than 1 mm, the thermal bimorph bending was not significant because the ethanol content was not sufficient to induce the transition of its shape. The bending curvature decreased as the thickness was increased above 2 mm. As the thickness of this elastomer matrix increased above the threshold, this sample became more resistive to bending (see The Blocked Moment section in the Supplementary Data). Regarding these factors, the soft actuator with a thickness of 2 mm was chosen because of its high bending curvature and fast response time.

For the electrothermal actuation of the bimorph actuators that were 2 mm thick, the soft actuator was made of the patterned heater based on a flexible film and a soft actuator segment. Figure 2a shows the mechanism of bimorph bending induced by the electrothermal energies. The bimorph bending was achieved due to the difference in the coefficient of thermal expansion (CTE) between a flexible heater film (CTE: 15×10^{-6}/°C) and a soft actuator segment. In our robotic system, the volume of the flexible heater film increased by 0.18% when it was heated from room temperature (25°C) to 150°C. In contrast, the expansion of the volume of the thermally responsive soft actuator was 208%. Due to the significant difference in their CTEs, the tensile strain was imposed mostly on the soft actuator segment, and this strain caused the soft robotic system to bend.

Figure 2b shows a photograph of the soft robotic system during its actuation. The flexible heater was attached to the right side of a soft actuator by applying an elastomeric adhesive (Ecoflex 5) that had a curing time of 5 min at room temperature. Figure 2c shows a plot of the effect of the heating temperature on the bending radius and strain of the soft actuators. Actuation began when the temperature of the flexible heaters was about 80°C, which corresponded to the temperature at which ethanol boils. When the temperature of heaters reached 150°C, the bending radius of the soft actuator was 30 mm. When the temperature was increased to more than 150°C, the bending radius remained at 30 mm, which possibly was due to the fact that the phases of all the microcapsules of ethanol were transformed from the liquid state to the gas state. In addition, the bending radius can be maintained statically and stably up to 30 min at the temperature of 150°C because the elastic restoring force is balanced by the expansion force of ethanol (related to its vapor pressure) at the temperature. The relevant data are added to Supplementary Figure S4. This controllability of bending curvature was advantageous in grasping soft and fragile objects.

Previously, this soft robotic system had the challenge of the vaporized ethanol capsules escaping from soft actuator frame, causing the degradation of the system's performance in repetitive actuation.[28] To enhance the reliability during repeated actuation, an anti-evaporation layer (Novec-1704; 3M) was coated on the surface of the soft actuators. This anti-evaporation layer consists of a hydrophobic fluoropolymer that prevents the escape of the ethanol vapors in the actuators.

Figure 2d shows the reliability of the soft actuators during repeated actuation. Without coating the anti-evaporation layer, the bending curvature was decreased dramatically due to the escape of the ethanol during eight repetitive actuation cycles. In contrast, by coating the anti-evaporation layer, the reliability of the soft actuators was enhanced to more than 1100 actuation cycles with negligible degradation. Figure 2e shows a schematic of the finger-like design of the soft actuator. The soft robotic finger was constructed from three electrothermally responsive soft actuator segments and two diced glasses as joints, which were designed to separately initiate the actuation of each segment as shown in Supplementary Video S1. Supplementary Figure S5 shows the characteristics of the patterned-flexible heaters for the finger's systems. The resistance of each individual electrode of the heater was 30–35 Ω. It was heated to 150°C at a current level of 100 mA. The methods that were used to fabricate the soft robotic fingers are described in the Materials and Methods section and illustrated in Supplementary Figure S6.

In addition to mimicking the locomotion of a person, it is important for the soft robotics to have the somatosensory function for rescue or detecting missions, and electric sensors are used to provide this function. For somatosensory functions, sensors are needed for sensing the pressure exclusively. However, the silicon field effect transistor-type (Si FET-type) pressure sensors[31,32] generate thermally excited carriers[33] since thermal energy is used to actuate our soft robotics. The integration of pressure and temperature sensors in parallel provides the somatosensory functions through the calibration step using the output signal of temperature sensors with the thermally induced output signals of the pressure sensors.

Figure 3a shows a schematic illustration and a photograph of the pressure-sensitive, finger-like soft actuator with a temperature sensor and a pressure sensor integrated in parallel above the surface of the flexible heater film. We integrated the flexible forms of heaters, soft actuator segments, and joints. Si FET-type pressure and temperature sensors were attached to the rightmost part of the flexible heater layer, where the object could be contacted. Figure 3b shows a schematic image of our pressure sensor and optical micrograph. In a pressure sensor, the Si FETs contain local air gaps

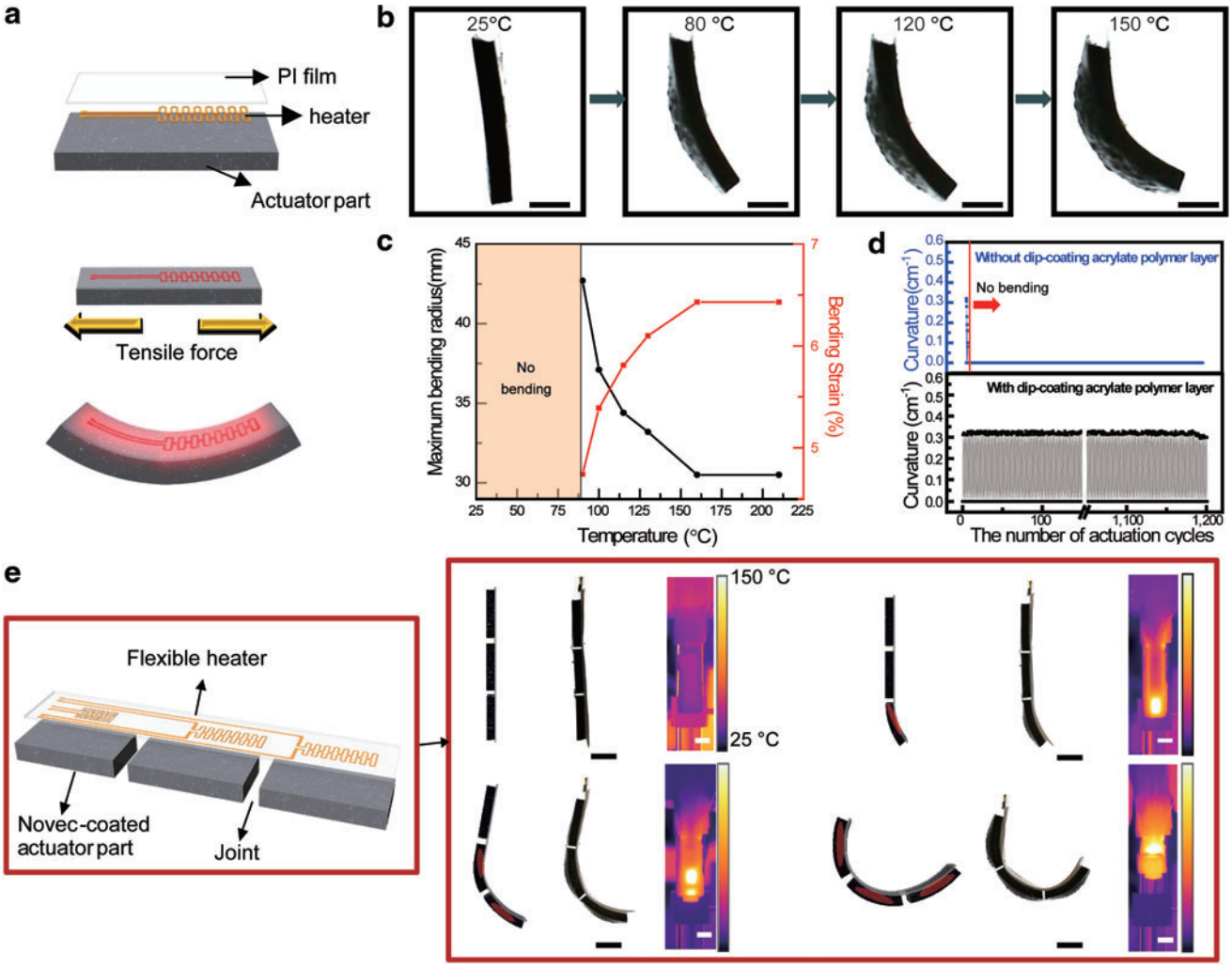

FIG. 2. Actuating properties of soft actuators. **(a)** The schematic illustrations of actuation mechanism. **(b)** Photographs of each actuation state over temperature increases. Scale bar, 5 mm. **(c)** The maximum bending radius and bending strain versus heating temperature of heater. **(d)** The comparison of reliability test results between pristine and anti-evaporation layer-coated soft actuators. **(e)** Schematic illustrations, photographs, and infrared images of the actuation of soft robotic finger. Scale bar, 10 mm. PDMS, poly(dimethylsiloxane); PI, polyimide; Si, silicon. Color images are available online.

as dielectric layers formed by 30-μm-thick elastomeric spacers (PDMS) between the top-gate and the source/drain electrodes.[34] The heights of the elastomeric spacers can be changed by applying pressure, thereby causing decreases in the thicknesses of the air gap layers. The decrease in the thickness ($\Delta d/d_0$) of the air gap layers can modulate the capacitance of the metal–air–Si structure, resulting in the detection of pressure ranges from 200 Pa to 5 MPa, as shown in Supplementary Figures S7 and S8. Figure 3c shows a schematic illustration of a temperature sensor and an optical micrograph. The temperature sensor is a field-effect transistor (FET) that uses a single-crystal Si channel. Electrons in the valence band are excited to the conduction band by increasing temperature. Therefore, the concentration of electron in the conduction band increases, and then, the drain current of the temperature sensor (FET) increases with temperature. The only difference between the pressure and temperature sensors is the materials of the spacers. The spacer of the air gap in the temperature sensor is a rigid, photo-patternable epoxy (SU-8; MicroChem Corp.) that is 30 μm thick; the height of the spacer is not changed by pressure. Thus, the drain current in the temperature sensor depends only on the temperature and is not dependent on the pressure. The methods used to fabricate sensors are described in the Fabrication of Pressure Sensor and Temperature Sensor section in the Supplementary Data. When the temperature of the heaters reached 150°C, the temperature of the pressure sensor was measured to about 66°C due to heat dissipation toward the soft actuator (Supplementary Fig. S9).

Figure 3d shows the pressure sensitivity of the pressure sensors integrated above the soft actuator at different temperatures as the contact force was increased from 0.75 to 750 kPa. The pressure sensitivity cannot be maintained because the thermally excited carriers affect the sensitivity of the sensors. Therefore, reliable feedback concerning the sensing of the pressures cannot be obtained. For somatosensory functions, a temperature sensor was integrated in parallel so that the temperature-induced current change in the

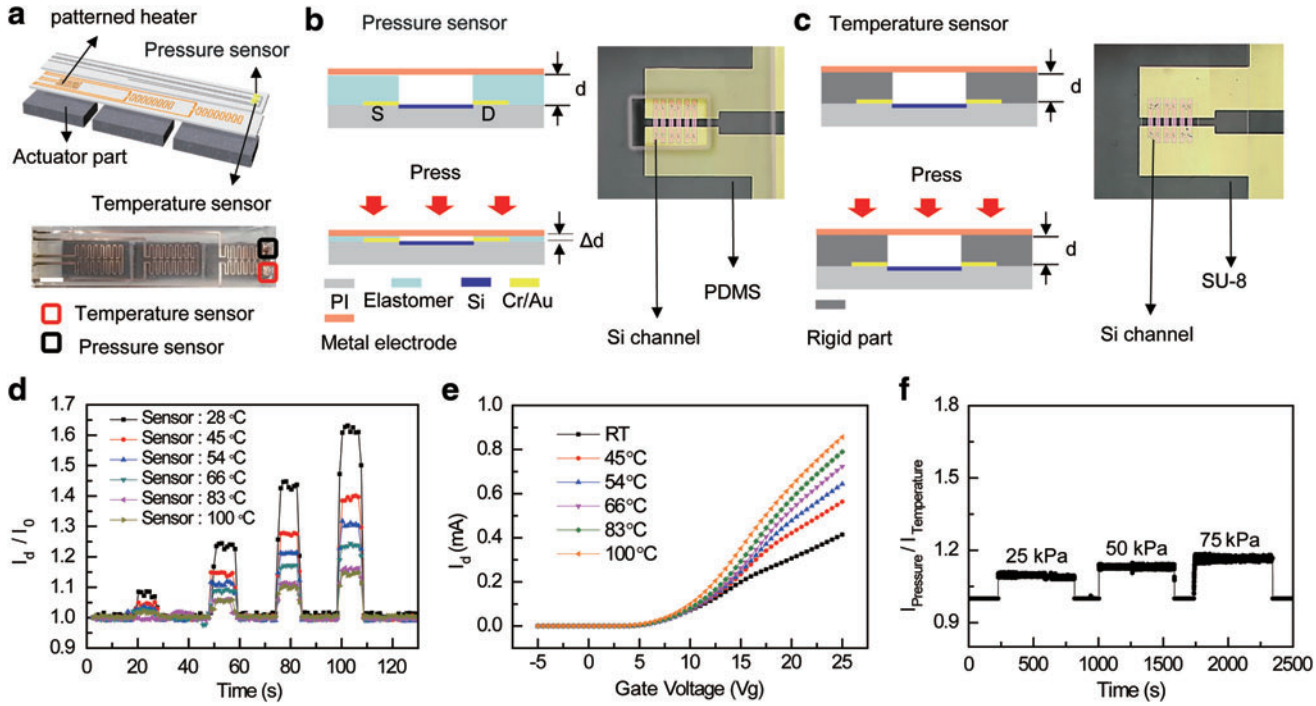

FIG. 3. Pressure-sensitive soft actuators. **(a)** The schematic illustration and photograph of the soft robotic finger, pressure, and temperature sensor. Scale bar, 10 mm. **(b)** Schematic illustrations and an optical micrograph of the pressure sensor. Scale bars, 150 μm. **(c)** Schematic illustrations and an optical micrograph of temperature sensor. Scale bars, 150 μm. **(d)** The plot of the pressure sensitivity of pressure sensor under different amounts of applied pressure with the increase in the temperature ($V_G = 25$ V and $V_D = 7$ V). **(e)** Transfer characteristics of temperature sensor based on silicon with increasing temperature ($V_G = -5$ to -25 V). **(f)** The plot of the pressure sensitivity characteristic by activating soft robotic finger (6 to 8 V; 80°C to 150°C) with calibration step. Color images are available online.

pressure sensor was calibrated. As a result, the output current of calibrated pressure sensor was not dependent on the temperature. Figure 3e shows the transfer characteristics of temperature sensors as the temperature of the heater increased in the range from room temperature to 100°C. Through the results of Figure 3d and e, the pressure-sensitive soft robotics are demonstrated in a way that mimics a person's sensory functions. When 25, 50, and 75 kPa of contact force of a soft robotic finger are imposed on the pressure sensors while actuating, the thermally induced signals of the pressure sensor are separated from the output signals of the temperature. Figure 3f shows the calibrated pressure sensing results. Supplementary Figure S10 shows the calibration steps of the output signal of a pressure sensor at different contact forces. To prove their resistance against repetitive actuation, the repetitive pressure-loading experiment was performed for more than 1100 cycles, after which it was ascertained that the degradation of the sensors was negligible (Supplementary Fig. S11).

In addition to the somatosensory function, respiratory functions can be obtained through the integration of the gas sensors with soft robotics. Figure 4a shows the variation of the sensor's signals from the Pd-coated SnO_2 NR arrays with time for various concentrations of H_2 (0–100 ppm). The gas sensors Pd-coated SnO_2 NR arrays on the front side of the film. The schematic illustration of the device layout for gas sensors is shown in Supplementary Figure S12. The inset of Figure 4a is a magnified plot of hydrogen sensing signals with time for low H_2 concentrations (0–10 ppm). Changes in the sensing signals of the Pd-coated SnO_2 NR arrays were not observed in the air sensing result. The sensing signal decreased from 10 s, and it was recovered at 16 s. Due to the limited volume of H_2 (1 mL), the sensing signal was recovered.

Figure 4b shows a schematic of the H_2 sensing mechanism of the Pd-coated SnO_2 NR arrays. The oxygen molecules in the air were adsorbed on the surface of the SnO_2 NR and ionized by taking electrons from the conduction band of the SnO_2 NR. Since the working temperature was below 150°C, the O^- and O^{2-} were adsorbed on the surface of SnO_2 NR, which led to the formation of the depletion layer. The adsorption rate of O^- of the Pd nanoparticles on the SnO_2 NR surface was enhanced due to the spillover effect.[35] The H_2 molecules decomposed into hydrogen atoms, and PdH_x was formed when the Pd-coated SnO_2 NR arrays were exposed to H_2. The hydrogen atoms reacted with O^- ions on the surface of the Pd-coated SnO_2 NR arrays. This induced changes in the resistance of the Pd-coated SnO_2 NR arrays due to the reduction of thickness of the depletion layer. The formation of PdHx induced the reduction of the Schottky barrier of the interface of the Pd nanoparticles and SnO_2 NR, and this led to the reduction of resistance. A more detailed hydrogen sensing mechanism of Pd-coated SnO_2 NR arrays can be found in previous reports.[36] The peak was located near 18 s for various concentrations of H_2. The sensor signal began to decrease at 10 s due to the reaction of the Pd-coated SnO_2 NR arrays with hydrogen. The limited volume of H_2 (1 mL) resulted in recovering the sensor's signal at 18 s. The changes in the

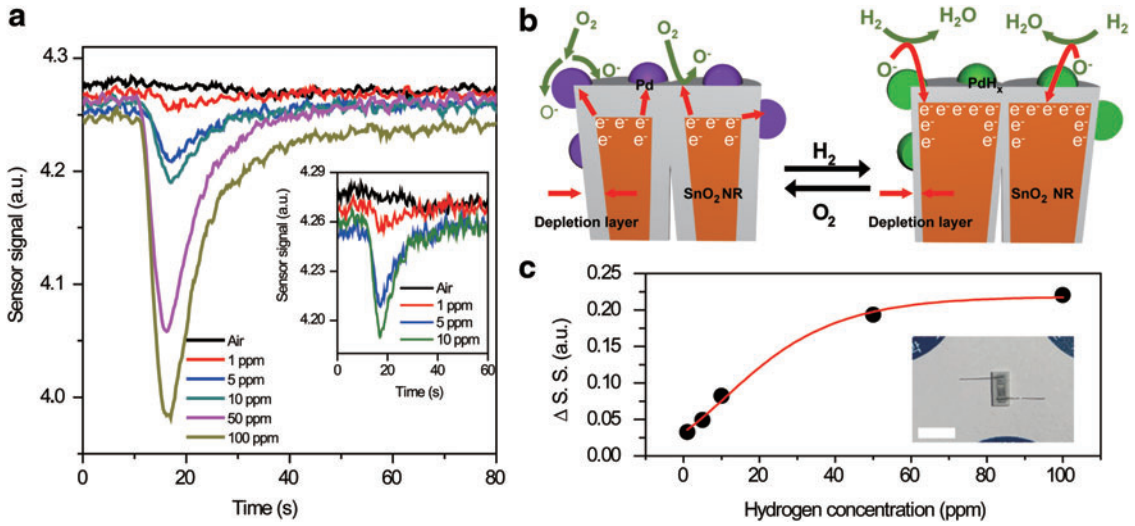

FIG. 4. Gas sensor properties for respiratory systems. **(a)** The plot of sensor signals of the Pd-coated SnO_2 NR arrays with time for various H_2 concentrations (0–100 ppm). **(b)** A schematic of H_2 sensing mechanism of the Pd-coated SnO_2 NR arrays. **(c)** The change in sensor signals was increased with the increasing H_2 concentration for various H_2 concentrations at 152°C. NR, nanorod. Color images are available online.

sensing signal were attributed to the change in the resistance due to the reaction of the Pd-coated SnO_2 NR arrays with H_2. Figure 4c shows that the change in the sensor signal was increased as the H_2 concentration increased for various H_2 concentrations. The inset of Figure 4c shows a photograph of our hydrogen sensor. The dimensions of the hydrogen sensor were 0.25×0.5 cm.

With the integrations of soft robotics with sensory functions, the untethered functions of soft robotics have attracted great interest in recent years for various applications. Although diverse researches on obtaining the somatosensory functions have been conducted, untethered soft robotic systems have not been commercialized successfully.[37–39] In our study, the untethered soft robotic systems provide an advanced concept on the IoT-based wireless technology. In our approach of demonstrating untethered soft robots, Figure 5a shows schematic images and a photograph of our hand-like soft actuator with wireless systems for sensing pressure and explosive gases. We integrated a Bluetooth module, power charging and supplying unit, current amplifiers, and sensing receiver units for pressure and gases on the frame of the body that was isolated from the soft body. The micro controller unit with a Bluetooth module (a Beetle Bluetooth Low Energy—Arduino Bluetooth 4.0) was used to convert the analog signals transmitted from a mobile phone to digital signals. The converted digital signals were transmitted to wireless temperature controllers and electric sensors. The power charging and supplying unit was used so that the power was supplied to the each of the modules for operation. The current amplifiers provided a high level of current amplified from input signals for increasing the temperature in the range of 25°C to more than 150°C. The sensing receiver units can supply digital signals to operate integrated electric sensors, and the output signals from the sensors can be received on the screen of a mobile device.

Figure 5b shows a photograph of our untethered soft robotic hand with the fully integrated wireless systems. The untethered soft robot with the wireless pressure sensing and actuating functions is demonstrated with grasping and releasing motions as shown in Supplementary Video S2. In Supplementary Video S2, the untethered soft robotic hand moves to different locations and then is actuated through wireless temperature controllers. When the soft robotic hand touches an object with 7.5g, the pressure sensing results are displayed on the screen of a smart phone. The maximum weight that this soft robotic hand can lift is 31.5 g (Supplementary Fig. S13). The colors displayed on the screen are dependent on the pressure intensities imposed on the pressure sensors. The pressure intensity range of green, yellow, and red colors is 1 to 25 kPa, 25 to 50 kPa, and to more than 50 kPa, respectively. In addition to wireless actuating and somatosensory functions, the wireless respiratory function is demonstrated.

Figure 5c shows photographs of the wireless actuation of the soft robotic hand with wireless gas and pressure sensing functions. Figure 5d shows the wireless real-time pressure sensing results, which were calibrated as shown in Supplementary Figure S14 while wirelessly sensing exposed hydrogen as shown in Figure 5e. For demonstration of somatosensory and respiratory functions, the customized chamber is used for preventing the leakage of gases. And, we used the hydrogen with 50 and 100 ppm for the wireless gas sensing function and an egg for the wireless pressure sensing function with the wireless actuating systems as shown in Supplementary Video S3. By pairing a smartphone with the customized application, the pressure that was detected and the gas sensing data were transferred wirelessly to the screen of a smartphone. The corresponding circuit diagram of our fully wireless systems is illustrated in Supplementary Figure S15. The relevant information on the estimated operation duration and communication distance of wireless components is described in The Operation Duration and Communication Distance of Wireless Components section in the Supplementary Data.

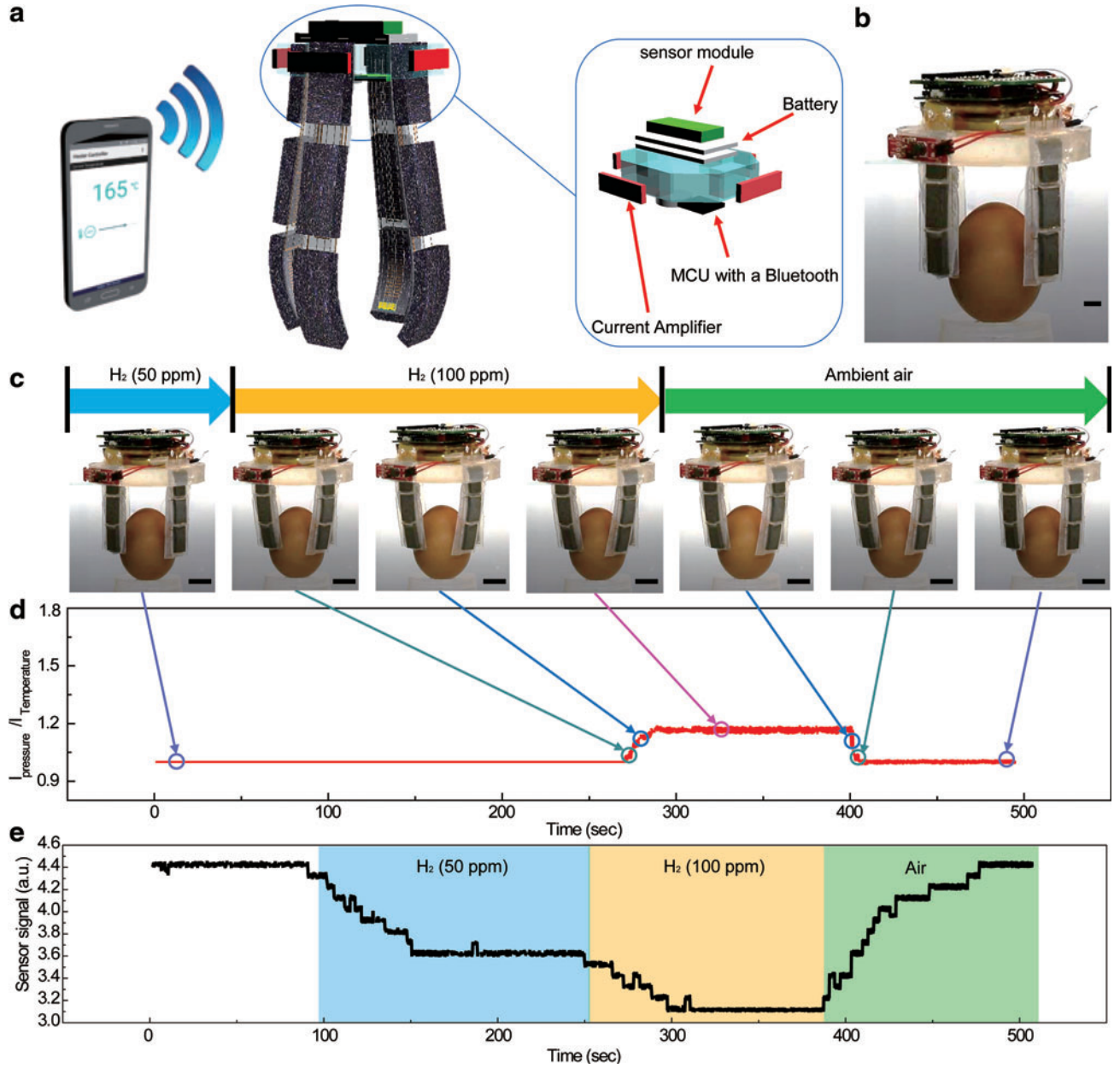

FIG. 5. Untethered soft robotic hands with integrated wireless systems for somatosensory and respiratory functions. **(a)** The schematic illustrations of wireless communicating systems between the smartphone and soft robotic hand. **(b)** The photograph of our untethered soft robotic hand with fully integrated wireless systems. Scale bar, 10 mm. **(c)** The photos of real-time operating moments of soft robotic hand. Scale bar, 20 mm. **(d)** The plot of wireless real-time pressure sensing results. **(e)** The plot of wireless hydrogen sensing with 50 and 100 ppm. MCU, microcontroller unit. Color images are available online.

Conclusions

In conclusion, we built and tested an electrothermally responsive, untethered soft robotic hand. The robotic hand included pressure, temperature, and gas sensors, a flexible heater, a power charging and supplying unit, a Bluetooth module, and an electronic circuit that provided wireless actuating and sensing systems for somatosensory and respiratory functions. The robotic hand was made of a thermally responsive elastomer composite in which microcapsules of ethanol and liquid metals were dispersed uniformly to form its shape and improve their uniformity of transition of shape and response rate for initiating of its actuation. Also, the repetitive actuating performance of this soft robot was optimized by controlling the fractions of ethanol and liquid metal by encapsulating them and using an anti-evaporation layer to prevent the loss of ethanol. The entire functions of this soft hand, including the gripping motion of the soft robotic fingers and the real-time detections of tactile pressures, temperatures, and hydrogen gas concentrations, were controlled wirelessly using a smartphone. Such an integration of soft actuators and sensors with fully flexible forms can overcome

the constraints associated with integrating soft robotic devices with conventional sensors that have rigid and fragile forms. Thus, this is a promising strategy for use in next-generation robotics that can sense their surroundings and function in harsh environments.

Author Disclosure Statement

No competing financial interests exist.

Funding Information

This work was supported by the Ministry of Science and ICT (MSIT) and the Ministry of Trade, Industry and Energy (MOTIE) of Korea through the National Research Foundation (2019R1A2B5B03069358 and 2016R1A5A1009926), the Bio and Medical Technology Development Program (2018M3A9F1021649), the Nano Material Technology Development Program (2015M3A7B4050308 and 2016M3A7 B4910635), and the Industrial Technology Innovation Program (10080577). Also, the authors thank financial support by the Institute for Basic Science (IBS-R026-D1) and the Research Program (2018-22-0194) funded by Yonsei University. In addition, W.L. was supported by the Basic Science Research Program through the National Research Foundation of Korea (NRF), and it was funded by the Ministry of Science, ICT and Future Planning (NRF-2017M3A9F1052297) and the Commercialization Promotion Agency for R&D Outcomes (COMPA) funded by the Ministry of Science and ICT (MSIT) (2019K000045).

Supplementary Material

Supplementary Data
Supplementary Table S1
Supplementary Figure S1
Supplementary Figure S2
Supplementary Figure S3
Supplementary Figure S4
Supplementary Figure S5
Supplementary Figure S6
Supplementary Figure S7
Supplementary Figure S8
Supplementary Figure S9
Supplementary Figure S10
Supplementary Figure S11
Supplementary Figure S12
Supplementary Figure S13
Supplementary Figure S14
Supplementary Figure S15
Supplementary Video S1
Supplementary Video S2
Supplementary Video S3

References

1. Shepherd RF, Ilievski F, Choi W, *et al.* Multigait soft robot. Proc Natl Acad Sci U S A 2011;108:20400–20403.
2. Liu F, Kim YB, Yee GK, *et al.* Computation of minimum contact forces of multifingered robot hand with soft fingertips. Intell Serv Robot 2015;8:225–232.
3. Rafsanjani A, Zhang Y, Liu B, *et al.* Kirigami skins make a simple soft actuator crawl. Sci Robot 2018;3:eaar7555.
4. Ainla A, Verma MS, Yang D, *et al.* Soft, rotating pneumatic actuator. Soft Robot 2017;4:297–304.
5. Miao Y, Dong W, Du Z. Design of a soft robot with multiple motion patterns using soft pneumatic actuators. IOP Conf Ser Mater Sci Eng 2017;269:012013.
6. Mosadegh B, Polygerinos P, Keplinger C, *et al*. Pneumatic networks for soft robotics that actuate rapidly. Adv Funct Mater 2014;24:2163–2170.
7. Carpi F, Kornbluh R, Sommer-Larsen P, *et al.* Electroactive polymer actuators as artificial muscles: are they ready for bioinspired applications? Bioinspir Biomim 2011; 6:045006.
8. Chen I-WP, Yang M-C, Yang C-H, *et al.* Newton output blocking force under low-voltage stimulation for carbon nanotube–electroactive polymer composite artificial muscles. ACS Appl Mater Interfaces 2017;9:5550–5555.
9. McKenzie RM, Barraclough TW, Stokes AA. Integrating soft robotics with the robot operating system: a hybrid pick and place arm. Front Robot AI 2017;4:39.
10. Polygerinos P, Wang Z, Galloway KC, *et al.* Soft robotic glove for combined assistance and at-home rehabilitation. Robot Auton Syst 2015;73:135–143.
11. Trivedi D, Rahn CD, Kier WM, *et al.* Soft robotics: biological inspiration, state of the art, and future research. Appl Bionics Biomech 2008;5:99–117.
12. Villanueva A, Smith C, Priya S. A Biomimetic robotic jellyfish (robojelly) actuated by shape memory alloy composite actuators. Bioinspir Biomim 2011;6:036004.
13. Qian X, Chen Q, Yang Y, *et al.* Untethered recyclable tubular actuators with versatile locomotion for soft continuum robots. Adv Mater 2018;30:1801103.
14. Lu X, Zhang H, Fei G, *et al.* Liquid-crystalline dynamic networks doped with gold nanorods showing enhanced photocontrol of actuation. Adv Mater 2018;30:1706597.
15. Kim J, Chung SE, Choi S-E, *et al.* Programming magnetic anisotropy in polymeric microactuators. Nat Mater 2011; 10:747–752.
16. Kwok SW, Morin SA, Mosadegh B, *et al.* Magnetic assembly of soft robots with hard components. Adv Funct Mater 2014;24:2180–2187.
17. Do TN, Phan H, Nguyen T-Q, *et al.* Miniature soft electromagnetic actuators for robotic applications. Adv Funct Mater 2018;28:1800244.
18. Acome E, Mitchell SK, Morrissey TG, *et al.* Hydraulically amplified self-healing electrostatic actuators with muscle-like performance. Science 2018;359:61–65.
19. Kellaris N, Venkata VG, Smith GM, *et al.* Peano-HASEL actuators: muscle-mimetic, electrohydraulic transducers that linearly contract on activation. Sci Robot 2018;3:eaar3276.
20. Yao S, Cui J, Cui Z, *et al.* Soft electrothermal actuators using silver nanowire heaters. Nanoscale 2017;9:3797–3805.
21. Wang C, Sim K, Chen J, *et al.* Soft ultrathin electronics innervated adaptive fully soft robots. Adv Mater 2018;30: 1706695.
22. Aia W, Xu Q. Overview of flexure-based compliant microgrippers. Adv Robot Res 2014;1:1–19.
23. Mavroidis C. Development of advanced actuators using shape memory alloys and electrorheological fluids. Res Nondestruct Eval 2002;14:1–32.
24. Liu C, Qin H, Mather PT. Review of progress in shape-memory polymers. J Mater Chem 2007;17:1543–1558.
25. Majidi C. Soft robotics: a perspective—current trends and prospects for the future. Soft Robot 2013;1:5–11.

26. Rus D, Tolley MT. Design, fabrication and control of soft robots. Nature 2015;521:467–475.
27. Rich SI, Wood RJ, Majidi C. Untethered soft robotics. Nat Electron 2018;1:102–112.
28. Miriyev A, Stack K, Lipson H. Soft material for soft actuators. Nat Commun 2017;8:596.
29. Bartlett MD, Kazem N, Powell-Palm MJ, *et al.* High thermal conductivity in soft elastomers with elongated liquid metal inclusions. Proc Natl Acad Sci U S A 2017;114:2143–2148.
30. Ford MJ, Ambulo CP, Kent TA, *et al.* A multifunctional shape-morphing elastomer with liquid metal inclusions. Proc Natl Acad Sci U S A 2019;116:21438–21444.
31. An BW, Heo S, Ji S, *et al.* Transparent and flexible fingerprint sensor array with multiplexed detection of tactile pressure and skin temperature. Nat Commun 2018;9:2458.
32. Shin S-H, Ji S, Choi S, *et al.* Integrated arrays of air-dielectric graphene transistors as transparent active-matrix pressure sensors for wide pressure ranges. Nat Commun 2017;8:14950.
33. Khanna VK. Temperature dependence of the electrical characteristics of silicon bipolar devices and circuits. In Extreme-Temperature and Harsh-Environment Electronics. Bristol, United Kingdom: IOP Publishing; 2017, pp. 1–4.
34. Jang J, Oh B, Jo S, *et al.* Human-interactive, active-matrix displays for visualization of tactile pressures. Adv Mater Technol 2019;4:1900082.
35. Morrison SR. Selectivity in semiconductor gas sensors. Sens Actuators 1987;12:425–440.
36. Kim MH, Jang B, Kim W, *et al.* Enhanced hydrogen sensing properties of Pd-coated SnO_2 nanorod arrays in nitrogen and transformer oil. Sens Actuators B Chem 2019; 283:890–896.
37. Kim H-J, Thukral A, Sharma S, *et al.* Biaxially Stretchable Fully Elastic Transistors Based on Rubbery Semiconductor Nanocomposites. Adv Mater Technol 2018;3:1800043.
38. Sim K, Rao Z, Kim H-J, *et al.* Fully rubbery integrated electronics from high effective mobility intrinsically stretchable semiconductors. Sci Adv 2019;5:eaav5749.
39. Sim K, Rao Z, Zou Z, *et al.* Metal oxide semiconductor nanomembrane–based soft unnoticeable multifunctional electronics for wearable human-machine interfaces. Sci Adv 2019;5:eaav9653.

Address correspondence to:
Jang-Ung Park
Department of Materials Science and Engineering
Nano Science Technology Institute
Yonsei University
Seoul 03722
Republic of Korea

E-mail: jang-ung@yonsei.ac.kr

Wooyoung Lee
Department of Materials Science and Engineering
Nano Science Technology Institute
Yonsei University
Seoul 03722
Republic of Korea

E-mail: wooyoung@yonsei.ac.kr